Part 2

Timing, General Relativity and Astrometry

Section D. Astrometry

https://doi.org/10.1017/S0252921100059261 Published online by Cambridge University Press

Pulsar Astronomy — 2000 and Beyond
ASP Conference Series, Vol. 202, 2000
M. Kramer, N. Wex, and R. Wielebinski, eds.

Pulsar Position, Proper Motion, and Parallax via VLBI

R.M. Campbell

Joint Institute for VLBI in Europe, Oude Hoogeveensedijk 4, 7991 PD Dwingeloo, the Netherlands

Abstract. I briefly review the means by which VLBI observations can determine the position, proper motion, and parallax of a pulsar, and consider a small subset of the applications of such results.

1. Introduction

Interleaved VLBI observations of a pulsar and one or more extragalactic reference sources that lie nearby on the plane of the sky can yield the position of the pulsar with sub-milliarcsecond uncertainties. A series of such observations well spread throughout the seasons can further yield the pulsar's position at a reference epoch ($\mathbf{r}_0$), its proper motion ($\boldsymbol{\mu}$), and its parallax (π) — the latter providing a model-independent distance. Combined with various other independent data, these results can be used to provide checks on models of n_e in the solar neighborhood, study the characteristics of plasma turbulence in the ISM (see, e.g., Gwinn, Bartel, & Cordes 1993), provide calibrations to scattering-based distance scales (Deshpande & Ramachandran 1998), investigate whether useful links may be established between individual pulsars and putative progenitors, estimate decay time scales for a pulsar's magnetic field, or determine frame ties between the extragalactic (Earth-rotation based) and dynamic (Earth-orbit based) reference frames (e.g., Bartel et al. 1996).

Previous VLBI pulsar astrometry based on phase modelling includes Gwinn et al. (1986), Bailes et al. (1990), and Bartel et al. (1996). A few new projects are using a phase-reference mapping approach (Chatterjee; Legge — both in these proceedings); Lestrade (1990, 1999) has pioneered such techniques on faint radio stars. Pulsar parallax can also be determined via ms-pulsar timing (Ryba & Taylor 1991), $\dot{P}_{\rm orb}$ and μ for binary ms-pulsars (Bell & Bailes 1996), and spectroscopic parallax for binary pulsars with a non-degenerate companion (Johnston et al. 1992). Here, I will briefly review how VLBI observations can provide an astrometric solution, illustrated with some sample results from our ongoing program, and discuss a small subset of the possible applications.

2. Estimation of Astrometric Parameters via VLBI

There are two stages in deriving a full astrometric solution ($\mathbf{r}_0, \boldsymbol{\mu}, \pi$): determining the pulsar's position with respect to known extragalactic reference source(s) at each observing epoch and calculating ($\mathbf{r}_0, \boldsymbol{\mu}, \pi$) from the set of these positions

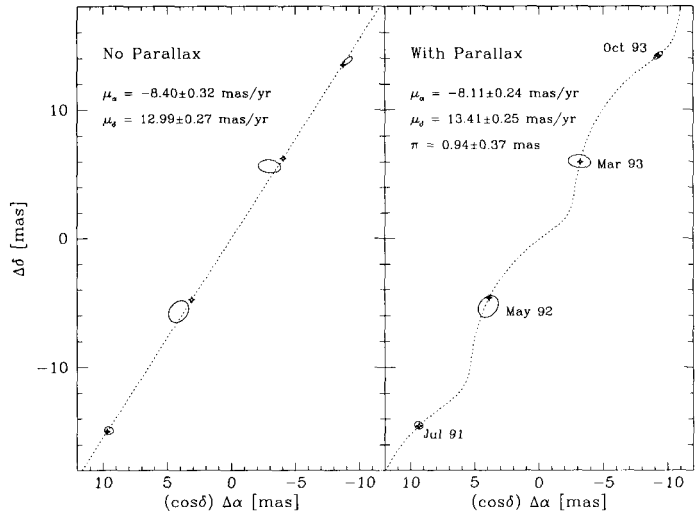

Figure 1. Positions of PSR B2021+51 at four epochs, represented by the error ellipses. The dotted line shows the modelled track of the pulsar's motion across the sky. The star-shaped points show the modelled position at the time of each observational epoch. Left panel: no parallax in model; right panel: parallax included in model.

at all epochs. We accomplish the first task essentially via modelling the total difference phase-delays between pairs of sources. Besides yielding the desired pulsar position, this allows investigation of its sensitivities to various other model parameters (such as station positions, Earth-orientation parameters, propagation factors, etc. — see, e.g., Guirado et al. 1995). For the second task, we simultaneously fit for $(\mathbf{r}_0, \boldsymbol{\mu}, \pi)$ in two dimensions using, from each epoch, the Earth's SSBC position taken from a planetary ephemeris and the pulsar positions, uncertainties, and correlations found above. By using the estimated correlation matrices in forming an input covariance matrix, we retain a maximum amount of information from the original observations in our final astrometric parameter estimates and correlations. The principal factors affecting systematic error include time-dependent structure in the reference sources, calibration of propagation effects, and assignment of the correct ambiguity lobe for the "connected" phases of one source with respect to another from a given station. Use of reference sources as close as possible to the pulsar (i.e., $<1°$ rather than $\sim 2\overset{\circ}{.}5$) helps mitigate the last two, and use of an array having baselines on all scales helps reduce vulnerability to the last. In any case, if we use two extragalactic reference sources per pulsar, preferably straddling it, any detected relative motion between them would set empirical limits on net systematic errors.

Figure 1 shows results from our program for four epochs for PSR B2021+51. Position uncertainties at each epoch were calculated conservatively, taking special account of the calculated sensitivity to the "ambiguity-lobe" assignment; if we used a more standard SNR-based procedure, the uncertainties in $\boldsymbol{\mu}$ and π would become 0.12–0.18 mas yr^{-1} and 0.19 mas, respectively. The larger uncer-

https://doi.org/10.1017/S0252921100059261 Published online by Cambridge University Press

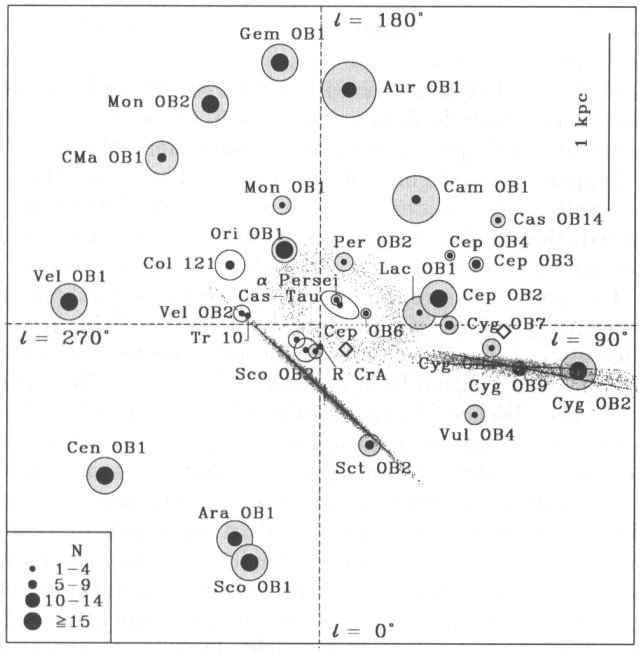

Figure 2. Monte Carlo birthplaces for PSR B1929+10 and PSR B2021+51 in relation to OB associations.

tainties in the middle two epochs stem from the loss of 1 or 2 stations from the original 6-station arrays. See Campbell (1995) and Campbell et al. (1996) for more details on the entire data-reduction procedure and these specific data.

3. Applications

The distance, together with the dispersion measure, allows estimation of a line-of-sight averaged electron density, $\langle n_e \rangle$. Let's consider two pulsars in roughly the same direction (lines of sight within $\sim 40°$ of each other) but at different VLBI-derived distances. PSR B2021+51 ($D = 1.06\,\mathrm{kpc}$) has $\langle n_e \rangle = 0.021 \pm 0.008\,\mathrm{cm}^{-3}$; PSR B1929+10 ($D \simeq 0.20\,\mathrm{pc}$) has $\langle n_e \rangle = 0.016 \pm 0.005\,\mathrm{cm}^{-3}$. Both compare well to the outer-disk component of the Taylor & Cordes (1993) n_e model in the vicinity of the Sun ($\simeq 0.019\,\mathrm{cm}^{-3}$) — but is the fact that the more distant pulsar has a higher $\langle n_e \rangle$ trying to suggest something about n_e variations in the local bubble (see, e.g., Ramesh Bhat et al.; Minter — both in these proceedings)?

An astrometric solution reduced to the pulsar's local standard of rest (LSR), plus an age estimate, allows tracing the pulsar's motion backwards through U_{gal} to a putative birthplace, subject to uncertainties in D (i.e., via σ_π), $\boldsymbol{\mu}$, and the unmeasured radial velocity (v_r). Figure 2 shows the loci of Monte Carlo birthplaces for PSR B1929 and PSR B2021 projected onto the Galactic plane, incorporating these three uncertainties as drawn from Gaussian distributions with the following means and standard deviations: $\mu_i' = \mu_i \pm \sigma_{\mu_i}$ (i.e., as estimated in

https://doi.org/10.1017/S0252921100059261 Published online by Cambridge University Press

the astrometric solution), $\pi' = \pi \pm 0.2$ mas (σ_π taken as constant to illustrate the scaling effect with D), and $v_r = 0 \pm v_t/\sqrt{2}$ (where v_t is the transverse velocity in the pulsar's LSR). The background is a map of OB associations in the solar neighborhood, taken from de Zeeuw et al. (1999) by permission. The diamonds mark our (current) VLBI positions for the pulsars (here, the loci of Monte Carlo birthplaces happen to lie roughly towards $\ell \sim 0$). The two darker linear loci for each pulsar result from considering the three sources of uncertainty separately (though plotted, the one due to σ_μ is too small to be seen at this scale). The one due to v_r lies parallel to the current Sun–pulsar direction, symmetric about the mid-point. The grey points represent the Monte Carlo birthplaces considering all three uncertainty sources simultaneously. I plot 3000 Monte Carlo trials in each case (see `www.nfra.nl/~campbell` for an easier-to-interpret color version of this plot). The contribution from σ_D scales with D, but the contribution from v_r does not; in the absence of any external information, this will dominate the net birthplace uncertainty for nearby pulsars. For $v_t \sim 100\,\mathrm{km\,s^{-1}}$, the magnitude of the two contributions are approximately equal at $\sim$1 kpc, as seen for PSR B2021. Although not done in this plot, the OB associations can also be traced backwards in time using Hipparcos data (de Zeeuw et al. 1999).

Conversely, an astrometric solution reduced to the pulsar's LSR, plus an assumed birthplace, allows calculation of a Monte Carlo estimate of the pulsar's kinetic age, τ_k. Comparison of τ_k with the spin-down age allows inference of the decay time scale of the pulsar's magnetic field. Drawing the assumed birthplace from an exponential distribution with a scale height of 60 pc (i.e., that of OB stars), the total uncertainty in the Monte Carlo τ_k is ~ 1.2 Myr, compared to a combined uncertainty from σ_D and v_r together of ~ 0.4 Myr. Some independent assumption about the birthplace would be required to obtain a more useful constraint on τ_k, and hence τ_D, for individual pulsars.

References

Bailes, M., Manchester, R. N., Kesteven, M. J., et al. 1990, Nature, 343, 240
Bartel, N., Chandler, J. F., Ratner, M. I., et al. 1996, AJ, 112, 1690
Bell, J. E., & Bailes, M. 1996, ApJ, 456, L33
Campbell, R. M. 1995, Ph.D. Thesis, Harvard University
Campbell, R. M., Bartel, N., Shapiro, I. I., et al. 1996, ApJ, 461, L95
Deshpande, A. A., & Ramachandran, R. 1998, MNRAS, 300, 577
Guirado, J. C., Marcaide, J. M., Elósegui, P., et al. 1995, A&A, 293, 613
Gwinn, C. R., Bartel, N. & Cordes, J. M. 1993, ApJ, 410, 673
Gwinn, C. R., Taylor, J. H., Weisberg, J. M., & Rawley, L. A. 1986, AJ, 91, 338
Johnston, S., Manchester, R. N., Lyne, A. G., et al. 1992, ApJ, 387, L37
Lestrade, J.-F., Rogers, A. E. E., Whitney, A. R., et al. 1990, AJ, 99, 1663
Lestrade, J.-F., Preston, R. A., Jones, D. L., et al. 1999, A&A, 344, 1014
Ryba, M. F., & Taylor, J. H. 1991, ApJ, 371, 739
Taylor, J. H., & Cordes, J. M. 1993, ApJ, 411, 674
de Zeeuw, P. T., Hoogerwerf, R., de Bruijne, J. H. J., et al. 1999, AJ, 117, 354